TU Delft
Challenging Glass 3 – Conference on Architectural and Structural Applications of Glass, Bos, Louter, Nijsse, Veer (Eds.), TU Delft, June 2012.

Experimental Investigations on Continuous Glass-GFRP Beams. Preliminary Non-linear Numerical Modelling

Luís Valarinho, João R. Correia, Fernando Branco
Instituto Superior Técnico/ICIST, Portugal, luis.valarinho@civil.ist.utl.pt
José Sena-Cruz
School of Engineering, University of Minho, Portugal, jsena@civil.uminho.pt

This paper describes results of experimental and numerical investigations about the structural behaviour of composite beams made of annealed glass panes and GFRP pultruded profiles. A brief description of flexural tests previously carried out on simply supported glass and glass-GFRP composite beams is first presented. Then, results of flexural tests on two-span glass-GFRP composite beams, bonded with three different structural adhesives, are described in detail. Finally, a preliminary numerical study of the glass-GFRP composite simply supported beams is presented. In this study, two-dimensional finite element models were developed in order to simulate and analyse the serviceability and post-cracking behaviour of those beams. Experimental and numerical results presented in this paper prove the advantages and technical viability of glass-GFRP composite beams.

Keywords: Glass-GFRP, Continuous beams, Numerical simulation, ductility

1. Introduction

Glass has played a central role on modern architecture since the 19th century, namely due to its many aesthetical possibilities combined with its main feature: transparency. Since then glass has had an important use on building façades. A few decades ago, glass has also started to be used as a structural material and there are already several examples of civil engineering applications in roofs, floors, beams and columns.

Structural elements made of float glass present several limitations, including relatively low tensile strength and brittle behaviour, which contrasts with the current design philosophies associated with more conventional materials, such as steel and reinforced concrete, for which ductility of structural members must be guaranteed.

The traditional alternatives to overcome the above mentioned limitations of float glass consist of using either toughened glass or laminated glass [1]. Toughened glass presents higher tensile strength compared with float glass, however it still exhibits a fully brittle behaviour at failure. On the contrary, laminated glass is capable of displaying a pseudo-ductile and redundant behaviour – if one of its glass panes cracks or breaks, polyvinyl butyral (PVB) films not only keep them in place but also transfer the tensile stresses to the other panes.

More recently, a different approach has been pursued by several authors (*e.g.*, [2-5]), which consists of joining glass panes to other structural materials, namely stainless steel, carbon fibre reinforced polymer (CFRP) laminates, glass fibre reinforced polymer (GFRP) rods, concrete, wood and steel. The underlying principle of those composite members is similar to that of reinforced concrete and relies on the stress transfer between the glass pane and the strengthening material used when the tensile strength of glass is attained.

This paper first describes the main results of an experimental programme about the structural behaviour of composite beams made of annealed glass panes and glass fibre reinforced polymer (GFRP) pultruded laminates. In a first stage of the experimental campaign, flexural tests on simply supported glass and glass-GFRP composite beams were carried out, in which the effects of the geometry of the GFRP strengthening elements and the type of adhesive used to bond them to glass panes were investigated. The main findings of these tests, already described in detail in [6], are briefly summarized here. The second stage of the experimental campaign, whose results are described in detail in this paper, included flexural tests on continuous two-span glass-GFRP composite beams with an I-section made of a glass web and GFRP flanges. In these tests, the serviceability (stiffness, cracking loads) and ultimate behaviour (failure loads, crack pattern, failure modes, force redistribution and ductility) of the beams was analysed and compared, allowing the evaluation of the potential advantages of the proposed glass-GFRP structural system and structural adhesives in hyperstatic members. The final part of this paper describes the numerical simulation of the simply supported beams tested. In particular, two-dimensional finite element models were developed using FEMIX software [7], in order to simulate and analyse the serviceability behaviour of glass-GFRP composite beams (prior to glass breakage), as well as their post-cracking behaviour. A multi-fixed smeared crack model, available in FEMIX computer program, was used. For now, the numerical investigations focused only on the beams in which the strengthening material was bonded to the glass beam with an epoxy adhesive. For these beams, test results showed that the epoxy adhesive provides a high level of shear interaction at the bonded interfaces – therefore, complete shear interaction was assumed in the numerical models. Experimental and numerical results are compared in terms of initial stiffness, cracking load and crack pattern.

2. Experimental programme

2.1. Test programme

The experimental programme included material characterization tests (to more information about these tests see Valarinho [8]) and flexural tests on (i) simply supported beams and (ii) continuous two-span beams.

2.2. Beam geometry, flexural test setup and procedure

The simply supported (SS) beams comprised the following three types of geometries: (i) rectangular reference glass beams, with a cross section of 12×100 mm^2, without GFRP reinforcement (SS-S series); (ii) rectangular composite beams (SS-R series), similar to the former but strengthened in the bottom edge with a GFRP pultruded laminate with a cross section of 12×10 mm^2; and (iii) beams with I geometry (SS-I series), composed of the same glass panes strengthened in the top and bottom edges

with GFRP flanges (cross section of $76 \times 10\ mm^2$) and angles (cross section of $30 \times 20\ mm^2$ with a thickness of 4.8 mm) - Fig. 1. In both rectangular and I-section simply supported beams, the GFRP profiles were adhesively bonded to the glass panes with a 2 mm thick layer of two different types of adhesives: an epoxy structural adhesive (EPa, Sikadur 330) and a high performance elastic gap-filling polyurethane adhesive (PUa, Sikaflex 265). All simply supported beams, with a span of 1.50 m, were tested in a symmetrically 4-point bending configuration with a load span of 0.50 m.. Unlike the I-beams (SS-I-EPa and SS-I-PUa), in both rectangular beams (SS-R-EPa and SS-R-PUa), in order to prevent lateral deformation, four pairs of vertical metal guides were symmetrically positioned throughout the span - the outer pairs were placed at the support sections while the inner pairs were 0.725 m apart themselves - Fig. 2. All beams were monotonically loaded until failure under load control, at approximate speeds of 27 N/s and 10 N/s for the glass beams and the composite beams, respectively.

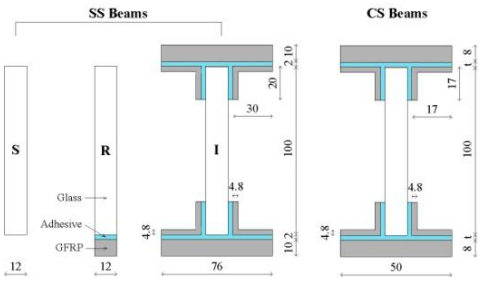

Fig. 1 - Geometry and cross section of beams from series S, R, I and I2 (dimensions in mm).

Fig. 2 - Experimental setup of the flexural tests on simply supported beams [6] (beam I-PUa).

For the continuously supported (CS) two-span beams only an I-section was tested, with a slightly different geometry than that used in the simply supported beams: the flange width was reduced to 50 mm – Fig. 1. A total of six beams were produced with the following three adhesives (2 beams of each type): (i) the polyurethane adhesive used in the simply supported beams (CS-I2-PUa); (ii) an alternative structural epoxy adhesive (Sikadur-31 cf, beams CS-I2-EPb); and (iii) an alternative polyurethane adhesive (Sikaforce 7710_L100, beams CS-I2-PUb). All interfaces were bonded with a 2 mm thickness layer of adhesive, except when PUb adhesive was applied – here, a 1 mm thickness was used given its low viscosity. The continuously supported beams, with two spans of L = 1.4 m, were tested in a 5-point bending configuration - Fig. 3. The load was applied using a 200 kN hydraulic jack reacting against a steel loading frame. A steel load distribution beam, placed between the jack and the tested beams, allowed applying a symmetrical point load distanced from the central support of 0.56 m (0.4 L, the configuration that ensures the maximum moment at the central support section and a ratio of 1.53 between the maximum negative and positive bending moments). In order to guarantee a symmetrical force distribution in both spans (in the linear stage), a steel roller was placed between the distribution beam and the hydraulic jack. In addition, to avoid any transverse loading, metal plates and spheres were placed between the distribution beam and the top surface of the tested beams. The supports consisted of cylindrical rollers, placed in-between metal plates. The central support was fully fixed, while the lateral supports allowed longitudinal sliding. In order to correct possible altimetry differences between supports, a thin layer of plaster was applied underneath

the supports, wherever needed. Support reactions and applied load were measured with load cells placed respectively below the supports (capacity of 50 kN in the outer supports and 100 kN in the central one; precision of 0.01 kN) and between the hydraulic jack and the distribution beam (capacity of 100 kN; precision of 0.01 kN). Displacements at the centre of each span were measured with displacement transducers (25 mm stroke; precision of 0.01 mm). Axial strains were measured throughout the depth of two cross-sections under negative and positive bending. All beams were monotonically loaded until failure under load control at an approximate rate of 130 N/s.

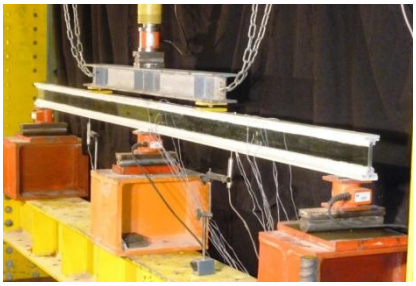

Fig. 3 - Experimental setup of the flexural tests on continuously supported beams (beam CS-PUb-2).

2.3. Materials

The beams tested comprised the following three different types of materials, whose properties are listed in Table 1: (i) 12 mm thick annealed glass panes, with edge treatment; (ii) GFRP laminates, made of an isophtalic polyester matrix reinforced with alternating layers of E-glass rovings and mats; and (iii) four different adhesives.

Table 1 – Mechanical properties, in tension, of the materials used on glass_GFRP beams (N.A. not available).

Material	σ_u [MPa]	E [GPa]	Source
Glass	58.9 ± 12.6	80.6	Testing (NP EN 1288-1:2007 and NP EN 1288-3:2007)
GFRP	475.5 ± 25.5	32.8 ± 0.9	Testing (ISO 527-1,4)
Epoxy Sikadur 330 (EPa)	22.5 ± 3.9	5.13 ± 0.11	Testing (ISO 527-1,4)
Polyurethane Sikaflex 265 (PUa)	3.4	(1.49 ± 0.22) × 10-3	Testing (ISO 527-1,4)
Epoxy Sikadur-31 cf (EPb)	18 to 24	5	Manufacturer
Polyurethane Sikaforce 7710_L100 (PUb)	13	N.A.	Manufacturer

3. Results of flexural tests

3.1. Flexural tests on simply supported beams

Results of flexural tests on simply supported beams (described in detail in [6]), are summarized in Fig. 4 (in Table 2 are presented the main results of I geometry simply supported beams), in which the load-deflection behaviour of the beams tested is illustrated. Results of this stage of the experimental programme, which included also

material characterization tests and tests on double lap joints between glass and GFRP adherends, allowed drawing the following main conclusions:

- The flexural tests proved the advantages and technical viability of glass-GFRP composite beams. In particular, it has been shown that it is possible to obtain relatively safe and ductile failure mechanisms in glass panes, provided that these are bonded to GFRP strengthening elements. In fact, after the development of the first crack in the glass pane, all strengthened beams kept their integrity, exhibiting a residual strength that varied with the type of adhesive and, as expected, with the geometry of the strengthening element (Fig. 4). In general, the load-deflection behaviour could be divided into two stages separated by the appearance of the first visible crack: on the first stage the behaviour was linear, given the mechanical characteristics of the main materials involved, while the second stage comprised a progressive loss of stiffness due to the damage progression on the glass pane, which ultimately led to the beam failure.
- In terms of post-cracking residual strength and ultimate load capacity, epoxy bonded composite beams presented much better performance than their polyurethane counterparts. For beams from series SS-R, even with a small strengthening cross-section, after glass cracking beam SS-R-EP was still able to fully recover the maximum load; in opposition, beam SS-R-PU did not present any post-cracking residual strength. In beams with I geometry, the strengthening cross-section increase augmented the post-cracking residual strength and both adhesives were able to mobilize a considerable residual strength (153% and 199% for beams SS-I-PU and SS-I-EP, respectively), providing significant safety levels. The ultimate strength of composite beams with epoxy adhesive was 1.37 and 3.95 times higher than that of beams with polyurethane adhesive in series SS-R and SS-I, respectively.
- In what concerns ductility, the fragile behaviour observed in the annealed glass beams was not repeated in none of the composite beams – these exhibited a pseudo-ductile behaviour after initial cracking, which, similarly to strength, varied with the strengthening geometry and, especially, with the type of adhesive. As expected, beams with polyurethane adhesive presented much higher ductility than beams with epoxy adhesive - the higher ductility of the former beams stemmed not only from the distribution of stresses between the two materials (also observed in the latter beams) but, essentially, from the high deformation capacity and low stiffness of the polyurethane adhesive, which caused significant slipping between the two materials. It should be mentioned, however, that the achievement of higher ductility levels had a counterpart, namely the lower values of initial stiffness, post-cracking strength and ultimate load capacity.
- The different types of adhesives led to different cracking patterns: beams with polyurethane adhesive had a cracking pattern characterized by few cracks, with a considerable spacing between them; beams with epoxy adhesive had a much more regular crack pattern (roughly similar to that exhibited by reinforced concrete beams), with vertical bending cracks in the central part of the beam and increasingly inclined shear cracks towards the supports along the shear span (Fig. 5).

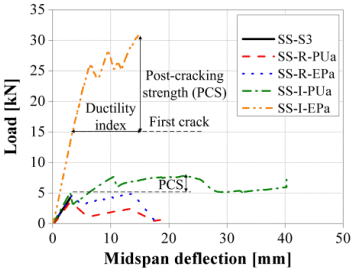

Fig. 4 - Experimental load *vs*. deflection curves from the simply supported beams [6].

Fig. 5 - Beam SS-R-EP: crack pattern in the brink of collapse [6].

3.2. Flexural tests on continuous two-span beams

Figures 6 to 9 summarize the experimental results obtained for the continuous beams in terms of the following parameters: (i) load *vs*. midspan deflection curves and strength (Fig. 6); (ii) distribution and variation of reactions and bending moments, both as a function of the applied load, in which the theoretical curves plotted were obtained from elastic force analysis; (iii) moment redistribution; and (iv) composite action. The results are presented separately for the different types of adhesives. The main results of the experimental tests on continuous beams are summarized in Table 2.

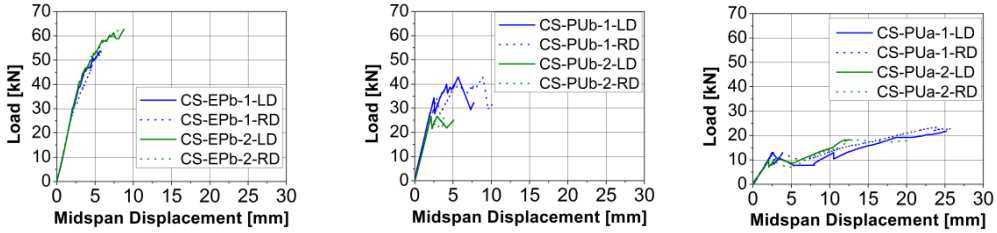

Fig. 6 - Load vs. midspan displacement of CS beams (LD – left span; RD – right span), from left to right, beams with EPb, PUb and PUa adhesives.

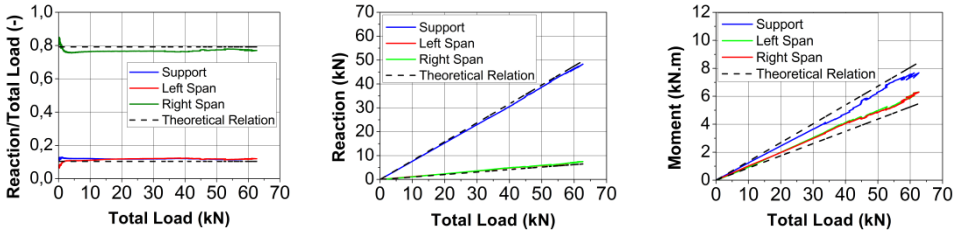

Fig. 7 - Load *vs*. distribution of reactions, load *vs*. variation of reactions and load *vs*. variation of bending moments of CS beams (only beam I-EPb is plotted).

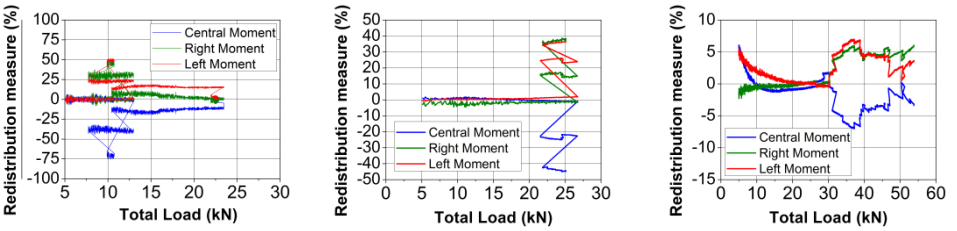

Fig. 8 - Load *vs*. redistribution of bending moments of beams, from left to right, CS-I-PUa-1 beam, CS-I-Pub-2 beam and CS-I-EPb-1.

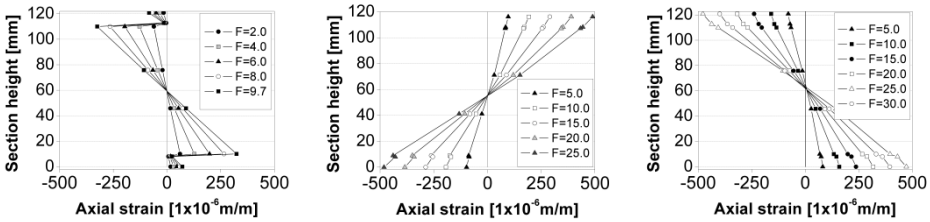

Fig. 9 – Axial strains *vs*. section depth for increasing total load [kN] of, from left to right, positive moment section on CS-I-PUa-1, negative moment section on CS-I-PUb-1 beam and positive moment section on CS-I-EPb-1CS beam (prior to glass cracking).

Figure 6 shows that the general load-deflection behaviour of the continuous beams was similar to that observed in the simply supported beams. Accordingly, there are two behavioural stages separated by the occurrence of the first visible crack. In the first stage all beams exhibited a linear behaviour with a similar stiffness in both spans. As expected, beams CS-I2-EPb exhibited the highest stiffness (14.5 kN/mm), followed by beams CS-I2-PUb (13.0 kN/mm), with the lowest stiffness being registered in beams CS-I2-PUa (5.05 kN/mm). The second stage was characterized by the propagation of cracks and by the corresponding progressive loss of stiffness, resulting in a pseudo-ductile behaviour.

With respect to the cracking load, as for stiffness, beams CS-I2-EPb and CS-I2-PUb presented the best performance, with cracking loads being more than two times higher than those of beams CS-I2-PUa. Although the average cracking load of CS-I2-EPb beams was slightly higher than that of the CS-I2-PUb beams, one of the beams of the latter series presented a higher cracking load than the average one registered on CS-I2-EPb beams. When the first visible crack developed, the midspan deflection of all beams was about 2.5 mm (L/585 of the span).

The crack pattern development was of two types: beams CS-I2-PUa exhibited few cracks that had a continuous development during the test and were particularly concentrated over the central support and on the loaded sections; on the remaining beams, the glass pane displayed a more distributed crack pattern. Those distinct behaviours can be attributed to the level of interaction at the bonded interfaces which, as discussed in [6], is low for the PUa adhesive and high for adhesives with higher stiffness, such as epoxy adhesives and Pub polyurethane. It is worth mentioning that all beams first cracked above the central support with the exception of one of the beams of CS-I2-EP2 series. In this beam the first crack appeared at the right midspan (most likely

due to material heterogeneity, as the bending moment in the support was higher); this occurrence can be noticed in the load *vs.* deflection curve at the right span, in which a premature loss of stiffness can be identified.

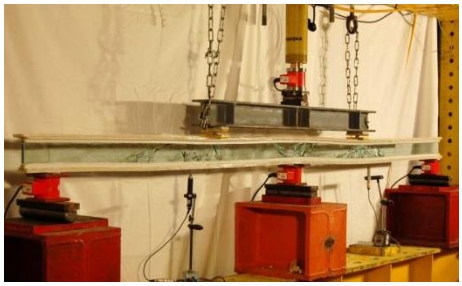

Fig. 10 – Cracking pattern of beams CS-I-PUa and CS-I-PUb-1

In the beams bonded with the PUb and EPb adhesives the failure modes were very similar and were caused by the sudden and explosive disintegration of the glass web (in most specimens, this only occurred in one of the spans – Fig. 11) after attaining a high level of damage with extensive cracking in the glass web. One of the beams with the PUa adhesive (CS-PUa-1) was unloaded without having collapsed (i.e., without web disintegration) after a considerable lateral (out of plane) deformation became visible, particularly in one of the loaded sections (Fig. 12). In the other beam of that series (CS-PUa-2), the test was not interrupted when such out of plane deformation began and the beam eventually failed due to a mechanism that involved lateral bending and crushing of the glass web below one of the loaded sections.

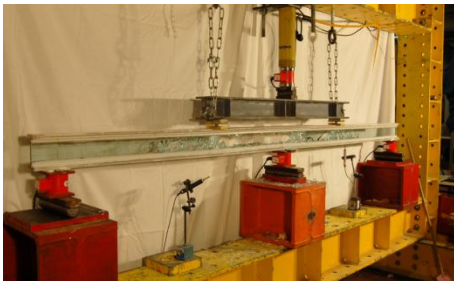

Fig. 11 - Failure mode of beam CS-I-PUb-1.

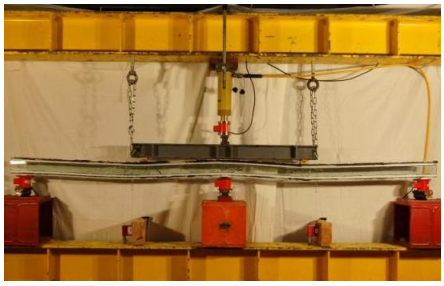

Fig. 12 – Deformation of CS-I-PUa beam prior to unloading.

Regarding the maximum load attained, it can be seen that the three types of beams behaved differently. Again, beams CS-I2-EPb presented the best performance attaining an ultimate load of 58.3 kN. The beams bonded with polyurethane adhesives presented much lower strength, especially beams CS-I2-PUa, with a failure load that was almost three times lower than that of beams bonded with epoxy. Beams CS-I2-PUb presented an intermediate strength of 34.8 kN. Despite the marked difference in terms of ultimate load between beams CS-I2-EPb and CS-I2-PUa, both types of beams presented a very similar post-cracking strength (ratio between ultimate load and cracking load) of 183%, indicating that a similar design philosophy can be used in those beams.

Unlike deflections at cracking, deflections at failure were very dissimilar for the different types of adhesives. Before unloading, beams CS-I2-PUa exhibited a deflection of 18.9 mm at the left midspan, a much higher deflection than that exhibited by beams CS-I2-EPb and CS-I2-PUb (6.4 mm and 8.6 mm, respectively). Consequently, the ductility index (defined as the ratio between the deflection at the first visible crack and the deflection at failure), was much higher in beams CS-I2-PUa (almost 1000%) than in the other beams (for the right span it was around 320% and 304%, respectively for beams CS-I2-PUb and CS-I2-EPb).

Table 2 - Summary of results of flexural tests on simply supported beams with I geometry and on continuous two-span composite glass-GFRP beams (average results are presented for series CS-I2-PUa and CS-I2-EPb).

Beam series	SS-I-PUa	SS-I-EPa	CS-I2-PUa		CS-I2-PUb		CS-I2-EPb	
Span	-	-	Left	Right	Left	Right	Left	Right
Initial stiffness (kN/mm)	1.74	4.55	5.05	5.01	13.5	12.7	14.7	14.1
Cracking load (kN)	5.09	15.50	11.4		30.6		32.1	
Maximum load (kN)	7.80[a]	30.81	20.9		34.8		58.3	
Post-cracking strength (%)	153	199	183		110		180	
Deflection at first visible crack (mm)	3.00	3.53	2.27	2.34	2.31	2.42	2.21	2.30
Deflection at failure (or before unloading) (mm)	26.5[b]	14.9	18.89	22.97	6.42	7.75	8.56	7.01
Deflection in terms of span at first visible crack	500	425	616	599	605	579	632	608
Deflection in terms of span at failure	57	101	74	61	218	181	164	200
Ductility index (%)	883	426	831	984	275	302	380	303

[a] Did not correspond to beam failure [b] Deflection at 80% of maximum load

The flexural tests on continuous composite beams also allowed analyzing the capacity of force redistribution between the central support and the loaded sections. The maximum bending moments at those sections and the corresponding maximum redistribution capacities are summarized in Table 3.

All beams were able to redistribute internal forces, following the damage propagation in their cross-sections. Yet, such capacity was different amongst the beams tested. It can be seen that beams CS-I2-PUa presented by far the highest redistribution capacity in line with their highest ductility index, compared with beams bonded with adhesives PUb and EPb. This result is consistent with the differences in the mechanical properties of PUa adhesive and the two other adhesives (PUb and EPb), and the influence of such properties on the ultimate strength of the beams (and also on the maximum moment and the redistribution capacity). Beams CS-I2-PUb and CS-I2-EPb, despite having similar values of ductility index, showed considerably different redistribution capacities, with beams CS-I2-PUb exhibiting higher capacity than beams CS-I2-EPb. Further studies

will be developed within this project (namely tests on adhesively bonded glass-GFRP joints) in order to understand better the reasons for such differences.

Since the redistribution of moments is a consequence of the loss of stiffness on several sections (due to the damage increase) and, in this case, is not due to the mechanical behaviour of the materials (as in steel or reinforced concrete structures), the moment redistribution from the central support to the spans was only momentarily observed, most of it occurring after the appearance of the first crack. With the development of the crack pattern and with the appearance of cracks in the spans, the beams had the tendency to re-equilibrate the force distribution, approaching the original elastic one – Fig. 8.

Table 3 - Results for failure behaviour of continuous two-span composite glass-GFRP beams.

Beam	Ultimate load (kN)	Maximum moment (kN.m)			Ductility index[a] (-)	Maximum redistribution (%)	
		Left	Support	Right		Support	Span
CS-I2-PUa-1	23.5	2.57	2.49	2.46	988%	-75%	52%
CS-I2-PUa-2	18.3	2.07	2.18	2.34	810%	-59%	15%
CS-I2-PUb-1	26.7	3.05	3.49	3.16	221%	-45%	39%
CS-I2-PUb-2	42.9	5.00	4.27	4.91	356%	-27%	28%
CS-I2-EPb-1	53.8	5.46	5.90	5.56	269%	-7%	7%
CS-I2-EPb-2	62.7	6.30	7.68	6.31	414%	-5%	9%

[a] average from both spans

4. Numerical simulation

4.1. Initial considerations

Smeared crack models have been used for the simulation of concrete in tension since the 1970s. In these models, the fracture process is initiated when the maximum principal stress in a material point exceeds its tensile strength. The propagation of the cracks is mainly controlled by the shape of the tension-softening constitutive law and fracture energy of the material. Normally, the mesh objectivity is guaranteed by associating the dissipated energy in crack propagation process with a characteristic length of the finite element. In order to avoid snap-back instability, the mode I fracture energy must be greater than a threshold value which depends on the tension-softening constitutive law. Typically, the fracture propagation in mode II is based on the concept of shear retention factor [9].

The numerical investigations described in this section comprised a parametric study carried out with the aim of evaluating the applicability of smeared crack models for the simulation of annealed glass structural elements strengthened with GFRP using an epoxy adhesive. For that purpose a multi-fixed smeared crack model [9] was selected from the FEMIX computer code, which is a general tool for the analysis of structures by the Finite Element Method [7]. The main analysed parameters were the fracture energy and the shear retention factor.

4.2. Description of the FE model

The strengthened beam SS-R-EPa was modelled as a plane stress problem. Fig. 13 shows the geometry, mesh, support conditions and load configuration used to develop the parametric study. To simulate the glass and GFRP, 4-node Serendipity plane stress elements were used with 2×2 Gauss-Legendre integration scheme. Linear elastic behaviour under compression was adopted. Perfect bond was assumed between both materials. This assumption is corroborated by the experimental observations (c.f. section 3). The shape of the tension-softening law was assumed as linear. The crack band width was assumed equal to the square root of the area of the finite element in order to assure that the results are not dependent on the mesh refinement. In the multi-fixed smeared crack model used, for a specific integration point, a new crack is initiated when the maximum principal stress exceeds the uniaxial tensile strength, and the angle between the direction of the existing cracks and the direction of the maximum principal stress exceeds the value of a predefined threshold angle. In the present study the threshold angle was assumed constant and equal to 30°. A maximum of 2 cracks per integration point was allowed to arise.

As referred before, the parametric study analysed the influence of the fracture energy and the shear retention factor on the load *vs*. deflection at midspan relationship. The numerical responses were compared with the experimental one. Additionally, in some cases the crack patterns were also compared.

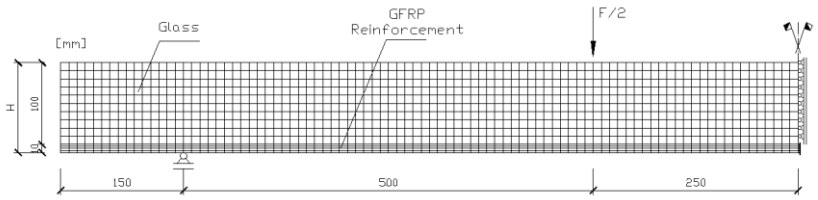

Fig. 13 – Mesh, support conditions and load configuration.

4.3. Results and discussion

For studying the effect of the mode I fracture energy (G_f) on the structural response of the annealed glass beam strengthened with GFRP, the following values were considered: $Gf_{,min}$, $1.5G_{f,min}$, $2.0G_{f,min}$ and $4.0G_{f,min}$, where $G_{f,min}$ is the minimum fracture energy required to avoid the snap-back instability [9]. According to the literature, the value of the glass fracture energy is about $G_{f,min}/100$ [1], although to the authors' best knowledge there is no experimental work reporting the determination of such value (3×10^{-3} J/m2). It is also worth mentioning the considerable scatter of G_f reported in other more conventional materials, namely concrete, for which differences of the same order of magnitude have been reported by several authors [10]. In the simulations of the present section the parameter p defining the shear retention factor was assumed to be equal to 2.0.

Fig. 14 depicts the relationships between the load and midspan deflection responses, both numerical and experimental. In this figure it can be seen that the simulation of the elastic branch matches the experimental response. With the exception of model "$4.0G_{f,min}$" all the numerical models predicted the crack load initiation. After this point a

sudden load decay is observed for model "$G_{f,min}$". This load decay is similar to the one observed in the experimental test. However, when the corresponding deflection is compared a large difference can be observed. This difference can be attributed to the fact that the data acquisition speed (1 Hz) was not fast enough to capture such drop in the experimental test. After this phase several cracks arose and then grew in terms of width and depth. At this stage, a similar response is observed for all the models (with the exception of model "$4.0G_{f,min}$"), which predicted quite well the experimental response including the failure load.

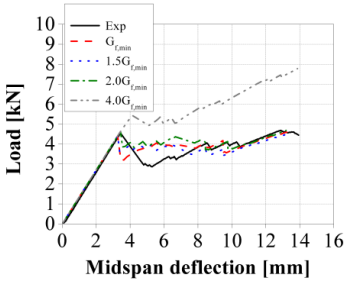

Fig. 14 – Effect of fracture energy on the load *vs*. mid-span deflection.

Fig. 15 presents the crack patterns obtained for different deflection levels of the models "$G_{f,min}$" and "$2.0G_{f,min}$". For all the stages analysed, the existing cracks are mainly "fully opened" (in purple), i.e. cracks where the mode I fracture energy is fully exhausted. In spite of model "$2.0G_{f,min}$" predicted a greater number of flexural cracks with higher depth, the model "$G_{f,min}$" showed a better similarity with the experimental observations in terms of crack pattern at the upper part of the strengthened beam. In addition, for both models, the horizontal cracks developing on the shear span at the GFRP vicinity can be perfectly identified in the experimental prototype.

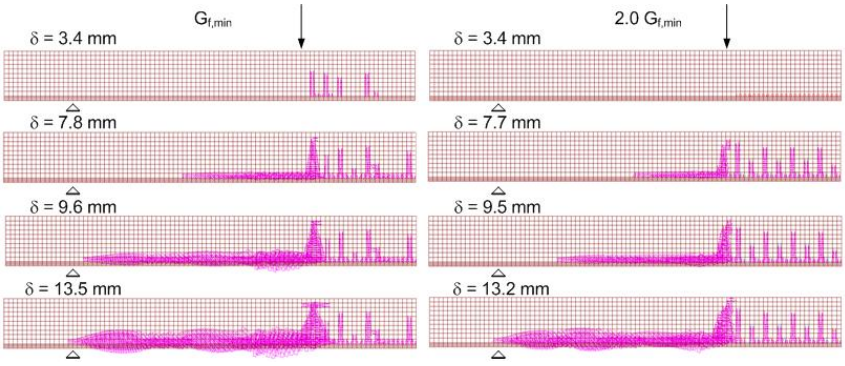

Fig. 15 – Effect of the fracture energy on the crack pattern, for the models with $G_{f,min}$ and $2.0G_{f,min}$.

The nonlinear material model used allows the evaluation of the shear retention factor, β, in two distinct ways [9]: (i) a constant value; (ii) a non-constant value defined by $\beta = (1 - \varepsilon_{cr}/\varepsilon_{cr,ult})p$, where ε_{cr} and $\varepsilon_{cr,ult}$ are the crack normal strain and the ultimate crack normal strain, respectively, and p is a parameter that can assume the values of 1, 2 or 3.

Figs. 16 and 17 show the influence of the shear retention factor on the structural response when the strategies (i) and (ii) are followed, respectively.

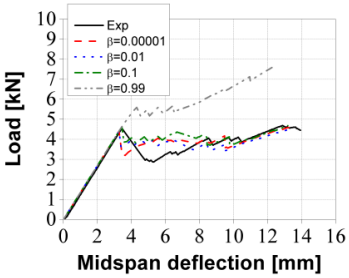

Fig. 16 – Effect of shear retention factor on the load vs. midspan deflection.

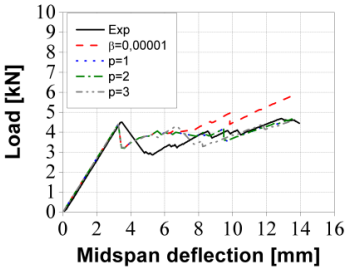

Fig. 17 – Effect of the parameter p on the load vs. midspan deflection.

In these simulations a linear tension-softening constitutive law was used and the fracture energy was assumed equal to $G_{f,min}$. When a fixed value for β is assumed (see Fig. 16), after crack initiation, the numerical models overestimated the experimental result. This behaviour was expected since during the crack propagation the numerical shear resistance degradation does not exist. When a non-constant value for the shear retention factor is adopted (see Fig. 17), the numerical model predicts quite well the overall response. Minimum differences were found for the cases of p=1, 2 and 3.

5. Conclusions

This paper presented results of experimental and numerical investigations on composite structural beams that combine annealed glass panes and GFRP pultruded profiles, the latter being used as strengthening elements and bonded to the former with different types of adhesives. The following main conclusions are drawn:

- The main advantage of the composite beams proposed in this study is their post-cracking residual strength and pseudo-ductility - the experimental tests on simply supported and continuously supported beams attested such better performance.
- The results obtained for the continuously supported beams were in line with the ones reported earlier for the simply supported beams - as expected, for similar adhesives, hyperstatic beams exhibited an increase of ultimate strength and a reduction of deflections.
- Amongst the continuous beams tested, the ones bonded with the PUa adhesive presented the highest values of ductility, much higher than those obtained for the other two types of adhesives, which were very similar to each other. Beams with PUa and EPb adhesives presented the highest post-cracking strengths, considerably higher than those exhibited by beams PUb. Although presenting similar values of post-cracking strength, as in the simply supported beams, the higher levels of ductility in beams PUa were obtained at the expense of lower values of initial stiffness, cracking and ultimate load.
- The redistribution capacities presented by the continuously supported beams were associated to the loss of stiffness of the cracked sections and were

strongly dependent on the type of adhesive – as expected, the highest force redistribution was obtained with the most deformable PUa adhesive. Due to the symmetry of the structural system and especially due to glass brittleness, the highest values of moment redistribution were only achieved momentarily, with the beams rapidly tending to re-equilibrate the distribution of internal forces.

- A numerical parametric study was performed with a multi-fixed smeared crack model that includes a linear tensile-softening law. The fracture energy and the shear retention factor were the main parameters analysed.
- The model with the minimum fracture energy required to avoid the snap-back instability, although being considerably higher than that referred in the literature for glass, predicted with high accuracy the main aspects observed experimentally, such as the crack initiation, stiffness degradation, load carrying capacity and crack patterns.
- According to the studies performed, the shear retention factor cannot be constant during the numerical test in order to include the shear degradation.

6. Acknowledgements

The authors wish to acknowledge FCT, ICIST and ADI (project n.º 3456/2009) for funding the research and companies SIKA, Guardian, STEP and ALTO for having supplied the adhesives, the glass panes and the GFRP pultruded profiles used in the experiments, respectively. The first author also thanks FCT for scholarship nº SFRH/BD/80234/2011.

7. References

[1] Haldimann M.; Luible A.; Overend M., *Structural Use of Glass*. Structural Engineering Documents 10, IABSE, Zurich, 2008.

[2] Louter P.C., *Adhesively bonded reinforced glass beams*, Heron 2007; 52: 31-58.

[3] Louter C.; van de Graaf A.; Rots J., Modeling the Structural Response of Reinforced Glass Beams using an SLA Scheme, Proceedings of Challenging Glass 2, Conference on Architectural and Structural Applications of Glass (eds. Bos, Louter, Veer), Delft, The Netherlands, 2010.

[4] Ølgard A.B.; Nielsen J.H.; Olesen J.F.; *Design of mechanically reinforced glass beams: modelling and experiments*, Structural Engineering International 2009; 19(2): 130-136.

[5] Louter C.; Leung C.; Kolstein H.; Vambersky J, Structural Glass Beams with Embedded Glass Fibre Reinforcement, Proceedings of Challenging Glass 2, Conference on Architectural and Structural Applications of Glass (eds. Bos, Louter, Veer), Delft, The Netherlands, 2010.

[6] Correia J.R.; Valarinho L.; Branco F.A., *Ductility and post-cracking strength of glass beams strengthened with GFRP pultruded composites*, Composite Structures 2011; 93(9): 2299-2309.

[7] Sena-Cruz, J.M.; Barros, J.A.O.; Azevedo, A.F.M.; Ventura-Gouveia, A., Numerical simulation of the nonlinear behavior of RC beams strengthened with NSM CFRP strips, Proceedings of the CMNE 2007 - Congress on Numerical Methods in Engineering and XXVIII CILAMCE - Iberian Latin American Congress on Computational Methods in Engineering, Abstract pp. 289, Paper nº 485 published in CD – FEUP, 20 pp., Porto, 13-15 June 2007.

[8] Valarinho, L., *Construction in structural glass: behaviour of glass–GFRP hybrid beams*, MSc Dissertation in Civil Engineering, Instituto Superior Técnico, Technical University of Lisbon, 2010.

[9] Sena-Cruz, J.M, *Strengthening of concrete structures with near-surface mounted CFRP laminate strips*, PhD Thesis, Department of Civil Engineering, University of Minho, 2004, 198 pp. URI: http://hdl.handle.net/1822/11781.

[10] Net, P.; Alfaiate, J.; Almeida, J.R.; Pires, E.B, *The influence of mode II fracture on concrete strengthened with CFRP*, Computers and Structures 2004; 82(17-19): 1495-1502.